Hindawi Publishing Corporation
International Journal of Antennas and Propagation
Volume 2016, Article ID 2474708, 14 pages
http://dx.doi.org/10.1155/2016/2474708

Research Article

Polarimetric Scattering from Two-Dimensional Dielectric Rough Sea Surface with a Ship-Induced Kelvin Wake

Pengju Yang and Lixin Guo

School of Physics and Optoelectronic Engineering, Xidian University, Xi'an 710071, China

Correspondence should be addressed to Pengju Yang; pjyang@yeah.net

Received 6 August 2015; Revised 17 December 2015; Accepted 20 December 2015

Academic Editor: Lorenzo Crocco

Based on the polarimetric scattering model of second-order small-slope approximation (SSA-II) with tapered wave incidence for reducing the edge effect caused by limited surface size, monostatic and bistatic polarimetric scattering signatures of two-dimensional dielectric rough sea surface with a ship-induced Kelvin wake is investigated in detail by comparison with those of sea surface without ship wake. The emphasis of this paper is on an investigation of depolarized scattering and enhanced backscattering of sea surface with a ship wake that changes the sea surface geometric structure especially for low wind conditions. Numerical simulations show that in the plane of incidence rough sea surface scattering is dominated by copolarized scattering rather than cross-polarized scattering and that under low wind conditions a larger ship speed gives rise to stronger enhanced backscattering and enhanced depolarized scattering. For both monostatic and bistatic configuration, simulation results indicate that electromagnetic scattering signatures in the presence of a ship wake dramatically differ from those without ship wake, which may serve as a basis for the detection of ships in marine environment.

1. Introduction

Fully polarimetric radars with four channels (HH, HV, VH, and VV) have advantages over the conventional single-polarization radar or dual-polarization radar when measuring ocean wave characteristics, since a fully polarimetric radar measures the entire scattering matrix, whereas a single-polarization radar or dual-polarization radar can only measure one or two elements of the scattering matrix. Ship-induced wake is of great value for the detection and classification of ships in marine environment, due mainly to the more distinct radar image signatures of ship-generated wake than ship itself. Much research effort has been devoted mainly to the extraction of specific information associated with ship from SAR images [1, 2] and to the radar imaging simulation of sea surface with ship-induced wakes [3–6]. The presence of ship-induced wake increases the roughness of sea surfaces under low wind conditions especially for a higher ship speed, and a larger sea surface roughness gives rise to a stronger multiple scattering. Fung and Eom investigated the multiple scattering and depolarization by Kirchhoff approximation and pointed out that the depolarized backscattering originates from multiple scattering [7]. Hence, it is of great value to investigate the fully polarimetric scattering including copolarized and depolarized scattering from sea surface in the presence of ship-induced wake.

Electromagnetic scattering from rough surface [8, 9] and rough surface with ship target on it [10–14] have been investigated extensively. However, fully polarimetric scattering from sea surface in the presence of ship-induced wake is rarely considered in the existing literatures, although copolarized (HH, VV) scattering from perfect electric conducting (PEC) sea surfaces with ship-induced wakes has been investigated in [15]. This is due mainly to the complexity of geometric modeling of sea surface with ship-generated wake as well as the corresponding fully polarimetric scattering modeling, which is three-dimensional (3D) electrically large problem and is beyond the capability of numerical methods such as method of moments (MoM) [16] and finite-difference time-domain (FDTD) [17]. Also, significant computational burden increases, since electromagnetic scattering from sea surface in the presence of ship-induced wake involves the stochastic properties of sea surfaces and we thus have to resort to Monte Carlo simulation. Analytical approximate models can deal

with 3D electrically large problem but is limited to their validity domains [18]. Moreover, most of analytical approximate models cannot correctly predict the depolarization of wave scattering from rough surface. Among analytical approximate models, the Kirchhoff approximation [19–21] also known as the physical optics and the tangent plane approximation cannot correctly show distinct polarization dependence. The two-scale model [22, 23] also known as composite surface model underestimates the cross-polarized components due to the neglect of second-order Bragg scattering. The second-order small perturbation method (SPM) can predict the depolarization in the plane of incidence, but the validity domain of SPM is restricted to small roughness [24]. The first order small-slope approximation (SSA-I) to some extent can predict the depolarized scattering outside the plane of incidence but cannot predict the depolarization of wave scattering from rough surface in the plane of incidence [25, 26].

Voronovich and Zavorotny [27] pointed out that the depolarized scattering from rough sea surface arises from two effects. The first effect is a result of mutual transformation of the two linear polarization states caused by facets' tilts and the second one is due to the second-order Bragg scattering. The second-order small-slope approximation (SSA-II) takes into account the two effects and thus can predict the electromagnetic wave depolarization from rough ocean surface. Accordingly, SSA-II is used in this paper to predict the monostatic and bistatic polarimetric scattering from sea surface in the presence of ship-induced Kelvin wake. The major concern in the present study is to investigate the depolarized scattering and enhanced backscattering from rough sea surface in the presence of ship-induced Kelvin wake by comparison with single rough sea surface without ship's wake. The remainder of this paper is organized as follows. Section 2 briefly presents the modeling of sea surfaces in the presence of ship-induced Kelvin wake. The polarimetric scattering model of SSA-II with tapered wave incidence is briefly presented in Section 3. The numerical results of monostatic and bistatic polarimetric scattering from sea surfaces with and without ship's Kelvin wake are discussed and analyzed in Section 4. Section 5 concludes this paper.

2. Modeling of Sea Surface with Ship-Induced Kelvin Wake

The simulation of rough sea surface elevation is crucial for the modeling of electromagnetic scattering from rough sea surface. The linear sea surface instead of nonlinear sea surface is considered in the present study, since the nonlinearity of ocean waves mainly influences the Doppler spectrum of time-varying rough sea surface and the present study involves only the average scattering coefficient of sea surface. The linear superposition method, fractal theory, and spectral method are widely used in generating linear rough sea surface.

In the present study, the spectral method under spatially homogeneous and time-stationary hypothesis is used to generate rough sea surface by taking into account its high efficiency, since the procedure of generating rough sea surface can be realized by fast Fourier transformation. All of the components of the linear sea surface in Fourier domain are completely independent of random phases. This implies Gaussian statistics for the sea surface elevations and their derivatives. The spatial Fourier amplitude at any time t can be expressed as follows:

$$\begin{aligned} &A\left(\bar{k},t\right) \\ &\quad = \gamma\left(\bar{k}\right)\sqrt{S\left(\bar{k},\phi\right)\delta k_x \delta k_y}\exp\left(i\omega t\right) \\ &\qquad + \gamma\left(-\bar{k}\right)^{*}\sqrt{S\left(\bar{k},\pi-\phi\right)\delta k_x \delta k_y}\exp\left(-i\omega t\right), \end{aligned} \tag{1}$$

where $\bar{k} = (k_x, k_y)$ is spatial wave vector. $S(\bar{k},\phi)$ is the sea surface roughness spectrum. $\gamma(\bar{k})$ is a complex Gaussian random series with zero mean value and unit variance. The sampling interval along x direction is $\delta k_x = 2\pi/L_x$ which is determined by the Nyquist sampling criterion with L_x being the length of sea surface along x direction. Similarly, $\delta k_y = 2\pi/L_y$ with L_y being the length of sea surface along y direction. According to the gravity-capillary dispersion relation, the angular frequency ω is related to the spatial wavenumber $k = |\bar{k}|$ by $\omega = \sqrt{gk(1 + k^2/k_m^2)}$ with g being the gravity acceleration constant.

Then, the sea surface elevation ζ_{sea} at spatial potion $\bar{r}$ for time t can be expressed by

$$\zeta_{\text{sea}}\left(\bar{r},t\right) = \sum_{\bar{k}} A\left(\bar{k},t\right)\exp\left(i\bar{k}\cdot\bar{r}\right). \tag{2}$$

Equation (2) can be efficiently accomplished by inverse fast Fourier transformation. To ensure that $\zeta_{\text{sea}}(\bar{r},t)$ is real, $A(\bar{k})$ is required to satisfy the conjugate symmetry about the origin as follows:

$$\begin{aligned} A\left(k_x,k_y\right) &= A^{*}\left(-k_x,-k_y\right), \\ A\left(k_x,-k_y\right) &= A^{*}\left(-k_x,k_y\right). \end{aligned} \tag{3}$$

The sea surface roughness spectrum proposed by Elfouhaily et al. is used in the present study for generating sea surface, which consists of gravity waves spectrum and capillary waves spectrum and is expressed as [28]

$$S\left(k,\phi,U_{10}\right) = k^{-4}\left(B_L\left(k\right) + B_H\left(k\right)\right)\Phi\left(\phi\right), \tag{4}$$

where B_L and B_H denote the long-wave and short-wave curvature spectrum, respectively. The detailed expressions of B_L and B_H can be found in [28]. $\Phi(\phi)$ represents the angular spreading function and is chosen as follows:

$$\Phi\left(\phi\right) = \frac{1}{2\pi}\left(1 + \Delta\left(k\right)\cos\left(2\left(\phi-\phi_w\right)\right)\right), \tag{5}$$

where ϕ_w is the wind direction with respect to the radar line of sight and

$$\Delta(k) = \tanh\left(\frac{\ln 2}{4} + 4\left(\frac{c(k)}{c(k_p)}\right)^{2.5} + 0.13\left(\frac{u_f}{c(k_m)}\right)\left(\frac{c(k_m)}{c(k)}\right)^{2.5}\right), \tag{6}$$

where $c(k) = \sqrt{g(1+k^2/k_m^2)/k}$, $k_m = 370\,\text{rad/m}$, $c(k_p) = U_{10}/\Omega_c$ with Ω_c being inverse wave age, $c(k_m) = \sqrt{2g/k_m} \approx 0.23\,\text{m/s}$, and u_f is the friction velocity.

Based on the Michell thin ship theory combined with the classic theory of a ship's wave resistance with a ship being regarded as a rigid body moving in inviscid incompressible fluid, Zilman et al. derived an explicit asymptotic expression for ship-generated Kelvin wake in the far zone [6]. Here, we briefly present the main formulations associated with a ship's Kelvin wake.

To approximately simulate a ship's wake, a parabolic ship is used which depends on length L, beam B, and draft T:

$$f(x,y) = \pm\frac{B}{2}\left(1-\left(\frac{2x}{L}\right)^2\right) \quad \left(|x| \le \frac{L}{2},\ -T \le z \le 0\right). \tag{7}$$

The ship-generated elevation of the free surface ζ_{ship} is related to the fluid velocity potential by the following expression:

$$\zeta_{\text{ship}}(x,y) = \frac{U_s}{g}\frac{\partial\varphi_{\text{ship}}(x,y)}{\partial x}. \tag{8}$$

Zilman et al. derived the asymptotic expression for fluid velocity potential by using a parabolic ship depicted by (7) as follows:

$$\varphi_{\text{ship}}(x,y,z) = -\frac{16BL}{\pi}U_s\text{Fr}^6\,\text{Re}\int_0^\infty d\tau C(\tau,x)\exp(iy\tau), \tag{9}$$

where

$$C(\tau,x,z) = \left(1-e^{-\nu\alpha T}\right)\frac{\sin(\beta(\tau))-\beta(\tau)\cos(\beta(\tau))}{\alpha^{3/2}\sqrt{1/4+\tau^2/\nu^2}} \cdot\cos\left(x\nu\sqrt{\alpha(\tau)}\right)e^{z\nu\alpha}, \tag{10}$$

$$\alpha(\tau) = 0.5\left(1+\sqrt{1+\frac{4\tau^2}{\nu^2}}\right),\ \beta(\tau) = \frac{\sqrt{\alpha(\tau)}}{(2\text{Fr}^2)}.$$

$\text{Fr} = U_s/\sqrt{gL}$ is the Froude number. It should be noted that (8) combined with (9) is in the form inverse Fourier integral and can be efficiently calculated by using fast Fourier transformation.

The total wave elevation of the free surface is assumed as a superposition of wind-generated sea surface elevation ζ_{sea} and ship-induced free surface elevation ζ_{ship} as follows:

$$\zeta = \zeta_{\text{sea}} + \zeta_{\text{ship}}. \tag{11}$$

Figures 1(a) and 1(b) present ship-induced Kelvin wake elevation of free surface with ship speed $U_s = 3\,\text{m/s}$ and wind-generated sea surface elevation of free wave with wind speed $U_{10} = 3\,\text{m/s}$, respectively. Under a fixed wind speed $U_{10} = 3\,\text{m/s}$, the simulated sea surfaces with ship-induced wake are presented in Figures 1(c) and 1(d) for ship speeds $U_s = 3\,\text{m/s}$ and $U_s = 5\,\text{m/s}$, respectively. From Figure 1, we can observe that the sea surface geometric structure is changed due to the presence of ship-induced Kelvin wake. More precisely, the sea surface roughness becomes larger due to the existence of a ship's Kelvin wake, especially at low wind conditions. The electromagnetic scattering signatures from sea surface will be thus affected due to the presence of a ship's Kelvin wake, which will be examined in detail in what follows.

3. Polarimetric Scattering Model of SSA-II with Tapered Wave Incidence

The small-slope approximation (SSA) [29] theory consists of a basic approximation of the theory (SSA-I) and second-order corrections to it (SSA-II) and represents a systematic expansion of a scattering amplitude with respect to slopes of rough surface, which has been successfully applied to evaluate microwave scattering from rough sea surfaces [27, 30]. The SSA-I cannot predict the depolarization of wave scattering from rough surface in the plane of incidence due to the neglect of the second-order Bragg scattering but to some extent can predict the depolarized scattering outside the plane of incidence. In comparison with the classical model such as SPM, KA, and TSM, the modern analytical approximate model of the SSA-II takes into account the mutual transformation of the two linear polarization states caused by facets' tilts and the second-order Bragg scattering and thus can predict the electromagnetic wave depolarization from rough ocean surface both in and outside the plane of incidence. In this paper, the SSA-II model is used to evaluate the monostatic and bistatic polarimetric scattering from two-dimensional (2D) dielectric rough sea surface with and without a ship's Kelvin wake to study the influence of a ship's Kelvin wake on the depolarized scattering and enhanced backscattering from rough sea surface.

The geometry of electromagnetic scattering from 2D sea surface is illustrated in Figure 2. θ_i and ϕ_i denote the incident angle and incident azimuth angle, respectively, whereas θ_s and ϕ_s represent the scattering angle and scattering azimuth angle, respectively. The incident wave vector is $\overline{k}_i = \overline{k}_0 - q_0\hat{z}$ and scattering wave vector $\overline{k}_s = \overline{k} + q\hat{z}$ can be decomposed into their horizontal projections and vertical components, respectively.

In this paper, a tapered plane wave is chosen as the incident field to reduce the edge effect caused by the limited

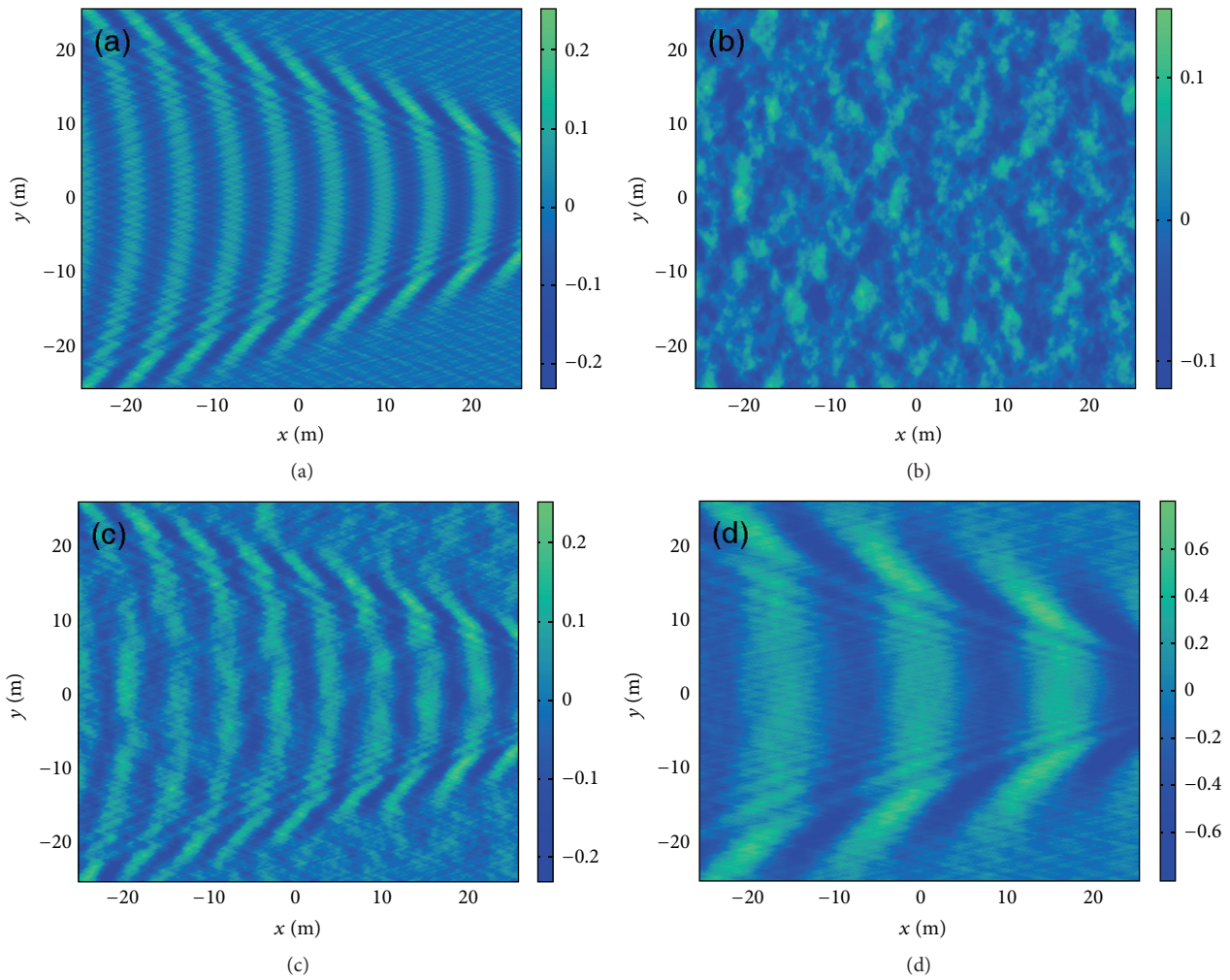

FIGURE 1: Simulated ship-induced Kelvin wake, wind-generated sea surface, and wind-generated sea surface with ship-induced Kelvin wake. (a) Ship wake only with ship speed $U_s = 3$ m/s, (b) sea surface only with wind speed $U_{10} = 3$ m/s, (c) ship-induced wake embedded in sea with $U_{10} = 3$ m/s and $U_s = 3$ m/s, and (d) ship-induced wake embedded in sea with $U_{10} = 3$ m/s and $U_s = 5$ m/s. The unit of the color bar is meter.

surface size of $L_x \times L_y$, and the tapered incident wave can be expressed as [31]

$$\begin{aligned} \overline{E}_i(\overline{r}) &= T(\overline{r}) \exp\left(i\overline{k}_i \cdot \overline{r}\right), \\ T(\overline{r}) &= \exp\left[i\left(\overline{k}_i \cdot \overline{r}\right) w\right] \exp\left(-t_x - t_y\right), \end{aligned} \tag{12}$$

where

$$\begin{aligned} t_x &= \frac{\left(x\cos\theta_i\cos\phi_i + y\cos\theta_i\sin\phi_i + z\sin\theta_i\right)^2}{g^2\cos^2\theta_i}, \\ t_y &= \frac{\left(-x\sin\phi_i + y\cos\phi_i\right)^2}{g^2}, \\ w &= \frac{1}{k_i^2}\left(\frac{2t_x - 1}{g^2\cos^2\theta_i} + \frac{2t_y - 1}{g^2}\right), \end{aligned} \tag{13}$$

and g is the parameter that controls the tapering of the incident wave. Thus, the original scattering amplitude of the SSA-II model can be expressed as follows after introducing into the tapered incident wave:

$$\begin{aligned} S\left(\overline{k}, \overline{k}_0\right) = {} & \frac{2\sqrt{q_0 q}}{\left(q_0 + q\right)\sqrt{P_{\text{inc}}}} \int \frac{d\overline{r}}{(2\pi)^2} T(\overline{r}) \\ & \cdot \exp\left[-i\left(\overline{k} - \overline{k}_0\right) \cdot \overline{r} + i\left(q + q_0\right) h(\overline{r})\right] \left(B\left(\overline{k}, \overline{k}_0\right)\right. \\ & \left. - \frac{i}{4} \int M\left(\overline{k}, \overline{k}_0; \overline{\xi}\right) h\left(\overline{\xi}\right) \exp\left(i\overline{\xi} \cdot \overline{r}\right) d\overline{\xi}\right), \end{aligned} \tag{14}$$

where P_{inc} is the incident wave power captured by the sea surface of limited size and

$$h\left(\overline{\xi}\right) = \frac{1}{(2\pi)^2} \int h(\overline{r}) \exp\left(-i\overline{\xi} \cdot \overline{r}\right) d\overline{r} \tag{15}$$

is the Fourier transformation of the surface elevation $h(\overline{r})$.

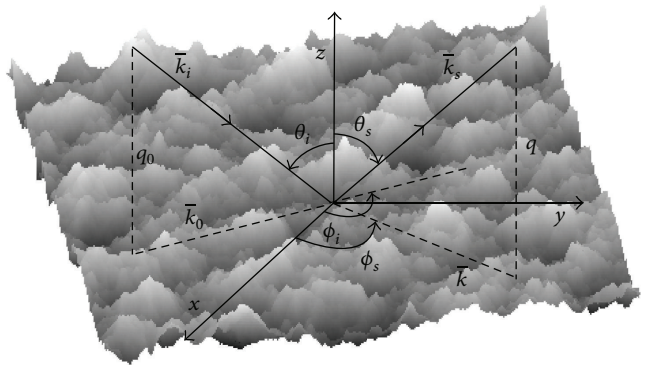

Figure 2: Geometry of 2D sea surface scattering problem.

The term $(i/4)\int M(\bar{k},\bar{k}_0;\bar{\xi})h(\bar{\xi})\exp(i\bar{\xi}\cdot\bar{r})d\bar{\xi}$ in (14) denotes the second-order correction to the first-order small-slope approximation, and (14) corresponds to first-order small-slope approximation by using $M(\bar{k},\bar{k}_0;\bar{\xi}) = 0$. It can be proven that, in a general case $M(\bar{k},\bar{k}_0;0) = 0$, and for this reason the term associated with $M(\bar{k},\bar{k}_0;\bar{\xi})$ in (14) is, in fact, proportional to the slopes of the rough surface rather than the elevations themselves. $M(\bar{k},\bar{k}_0;\bar{\xi})$ describes a contribution from the second-order Bragg scattering process and is related to the Bragg kernels B and B_2 by

$$M\left(\bar{k},\bar{k}_0;\bar{\xi}\right) = B_2\left(\bar{k},\bar{k}_0;\bar{k}-\bar{\xi}\right) + B_2\left(\bar{k},\bar{k}_0;\bar{k}+\bar{\xi}\right) + 2\left(q_0+q\right)B\left(\bar{k},\bar{k}_0\right), \tag{16}$$

where the kernel functions of B and B_2 are 2×2 matrices describing mutual transformations of the EM waves of different polarizations, which depend mainly on the polarizations, configuration angles, and the permittivity of the lower medium. The detailed derivation and corresponding kernel functions of the SSA model can be found in [29].

Based on the scattering amplitude calculated from small-slope approximation, the scattering coefficient is defined as

$$\sigma = 4\pi q_0 q\left\langle\left|S\left(\bar{k},\bar{k}_0\right)\right|^2\right\rangle, \tag{17}$$

where the angular bracket $\langle\cdot\rangle$ denotes the ensemble average over sea surface realizations. It should be noted that the scattering coefficient defined in this paper represents a total scattering coefficient including coherent and incoherent components. It differs from some literatures such as [25], in which only incoherent scattering component is considered with coherent component being neglected.

4. Numerical Results and Discussion

In the following simulations, the radar frequency is 1.2 GHz with a corresponding electromagnetic wavelength $\lambda = 0.25$ m. At the working frequency of 1.2 GHz, the relative complex permittivity of sea surface is $\varepsilon_r = 73.2 + i67.2$ at salinity of 30 parts per thousand and sea water temperature of 20°C in terms of Debye expression. The surface size is $L_x = L_y = 64$ m and the sampling interval is $\lambda/8$. The tapering parameter g is set to be $L_x/4$ to reduce the edge effect caused by the limited surface size. The wind fetch involved in Elfouhaily et al. spectrum is fixed at 30 km. The ship parameters are length $L = 50$ m, beam $B = 10$ m, and draft $T = 4$ m. The final monostatic and bistatic scattering is an ensemble average over 100 sea surface realizations. In all simulations, the radar is looking upwind.

To validate our small-slope approximation code, in Figures 3(a) and 3(b) we make a comparison of bistatic scattering coefficient obtained from SSA-I and SSA-II with that from MoM under incident angle $\theta_i = 60^\circ$ for wind speeds $U_{10} = 5$ m/s and $U_{10} = 10$ m/s, respectively. The sea surface is assumed to be one-dimensional and the length of sea surface is 204.8λ with λ being electromagnetic wavelength. Comparing the bistatic scattering coefficient calculated from SSA-I and SSA-II with that from MoM, we observe that SSA-II is in much better agreement with MoM compared to SSA-I. More precisely, for vertical polarization, both SSA-I and SSA-II are in rather good agreement with MoM. That is, SSA-II provides a small correction to SSA-I for vertical polarization. However, for horizontal polarization, the agreement between SSA-II and MoM is excellent but the difference between SSA-I and MoM is obvious. This means that SSA-II can provide more significant correction to SSA-I for horizontal polarization than for vertical polarization.

In Figures 4(a) and 4(b), we make a comparison of SSA-I and SSA-II for calculating the copolarized backscattering coefficient from 2D single rough sea surface and 2D sea surface with a ship's Kelvin wake embedded in it, respectively. The wind speed is $U_{10} = 3$ m/s and the ship speed is $U_s = 3$ m/s. By comparing the backscattering coefficient obtained from SSA-I with that from SSA-II, it is readily observed that SSA-II provides more significant correction to SSA-I for horizontal polarization than for vertical polarization. Moreover, the correction of SSA-II to SSA-I is much obvious for the sea surface with a ship's Kelvin wake than for a sea surface without a ship's Kelvin wake. The reason for this phenomenon is that ship's Kelvin wake makes the sea surface much rougher than the sea surface without a ship's Kelvin wake. By the way, there is no difference in the normalized Doppler spectrum of backscattered echoes from time-evolving rough surfaces, which is a much more precise and sensitive tool in assessing the scattering model's validity than the usual comparison of average scattering coefficient.

Figures 5(a) and 5(b) present the copolarized and cross-polarized backscattering coefficient from 2D rough sea surface with and without an embedded ship's Kelvin wake, respectively. The wind speed is $U_{10} = 3$ m/s and the ship speed is $U_s = 5$ m/s. Obviously, copolarized (HH, VV) backscattering coefficient is much larger than the cross-polarized (HV, VH) backscattering coefficient except for the larger incident angles. What is more, the backscattering coefficient for VV-polarization is always larger than that for HH-polarization and cross-polarization. This is attributed to the fact that the rough sea surface scattering is dominated by copolarized scattering rather than the depolarized scattering. Also, it is very interesting to note that HV-polarized backscattering coefficient is equal to VH-polarized one for the sea surface

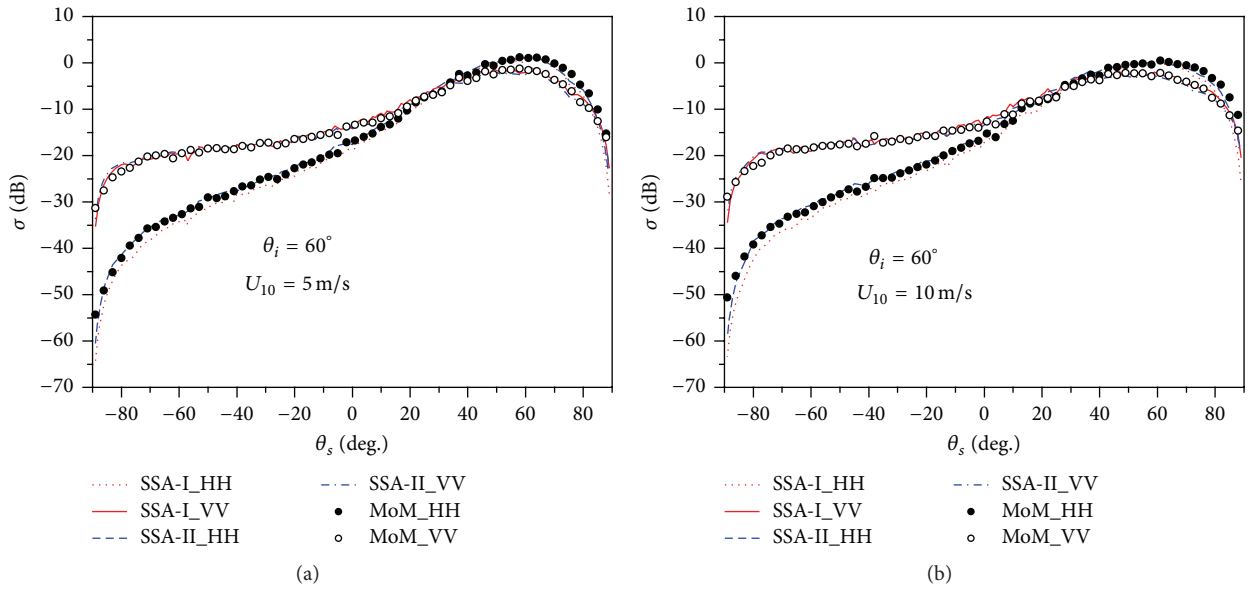

FIGURE 3: Validation of SSA by comparison with MoM for 1D case. (a) Wind speed $U_{10} = 5$ m/s and (b) wind speed $U_{10} = 10$ m/s.

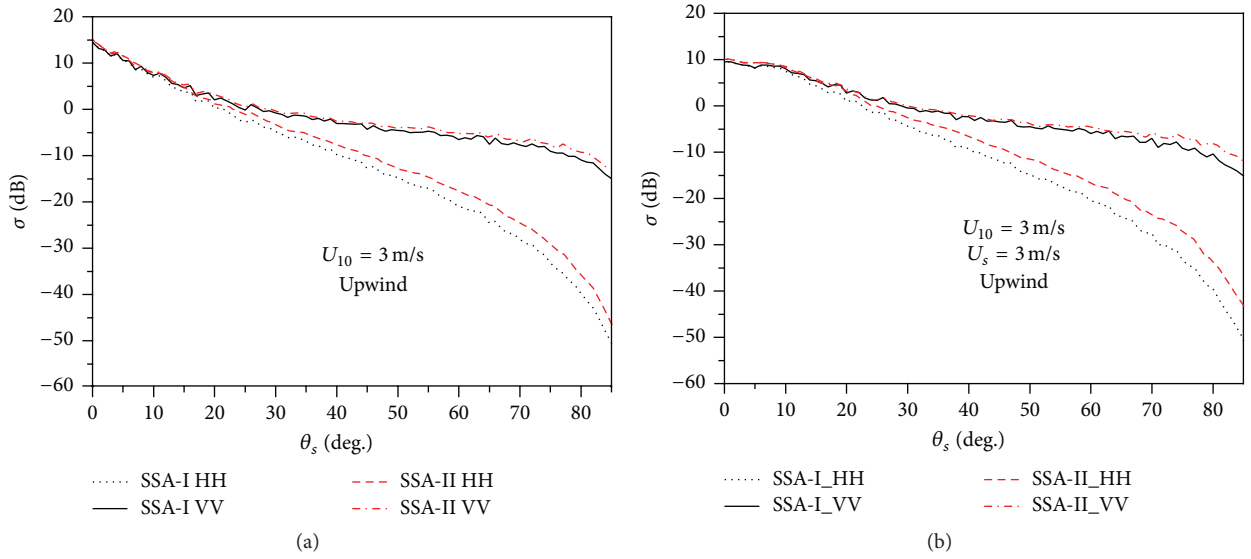

FIGURE 4: Comparison between SSA-I and SSA-II for copolarized backscattering coefficient with different wind speed $U_{10} = 3$ m/s. (a) Sea surface alone and (b) sea surface with wake.

with and without a ship's Kelvin wake embedded in it. This arises from the reciprocity which means that HV-polarized backscattering is equal to VH-polarized backscattering. On the other hand, the reciprocity of cross-polarized backscattering demonstrates the validity of SSA-II. By the way, the SSA-I cannot predict the depolarization of wave scattering from rough surface in the plane of incidence. Nevertheless, to some extent, SSA-I can predict the depolarized scattering outside the plane of incidence. In the present study, we used an Intel processor with 2.26 GHz CPU frequency and 32 GB memory. For backscattering scattering presented in Figure 5(a), the SSA-II takes about 24.6 hours and the SSA-I costs about 3.1 hours. Although SSA-I is much more efficient than SSA-II, it cannot predict the depolarization of wave scattering from rough surfaces in the plane of incidence. Thus, SSA-II instead of SSA-I is adopted in this paper to evaluate the polarimetric scattering from rough sea surface with or without a ship-induced Kelvin wake.

In Figure 6, the simulation condition is the same as Figure 5 but for wind speed $U_{10} = 10$ m/s. Comparing Figures 5(a) and 6(a), we can observe that, for sea surface without wake, the scattering intensity for wind speed $U_{10} = 10$ m/s in the vicinity of normal incidence is significantly decreased in comparison with that for wind speed $U_{10} = 3$ m/s. However,

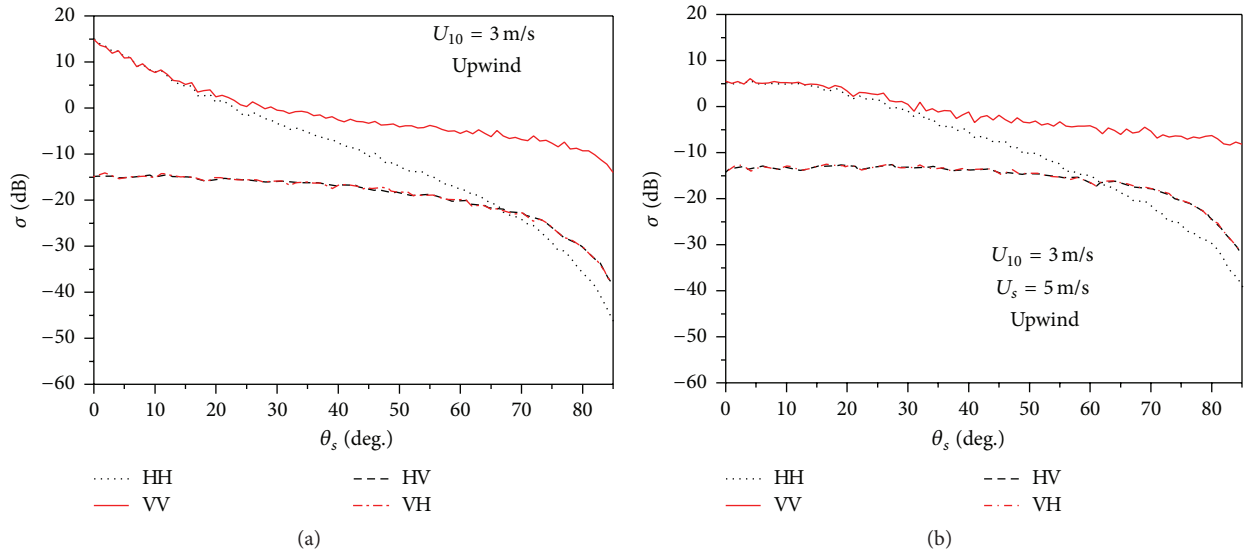

FIGURE 5: Comparison between copolarized and cross-polarized backscattering coefficient with wind speed U_{10} = 3 m/s. (a) Sea surface alone and (b) sea surface with wake at ship speed U_s = 5 m/s.

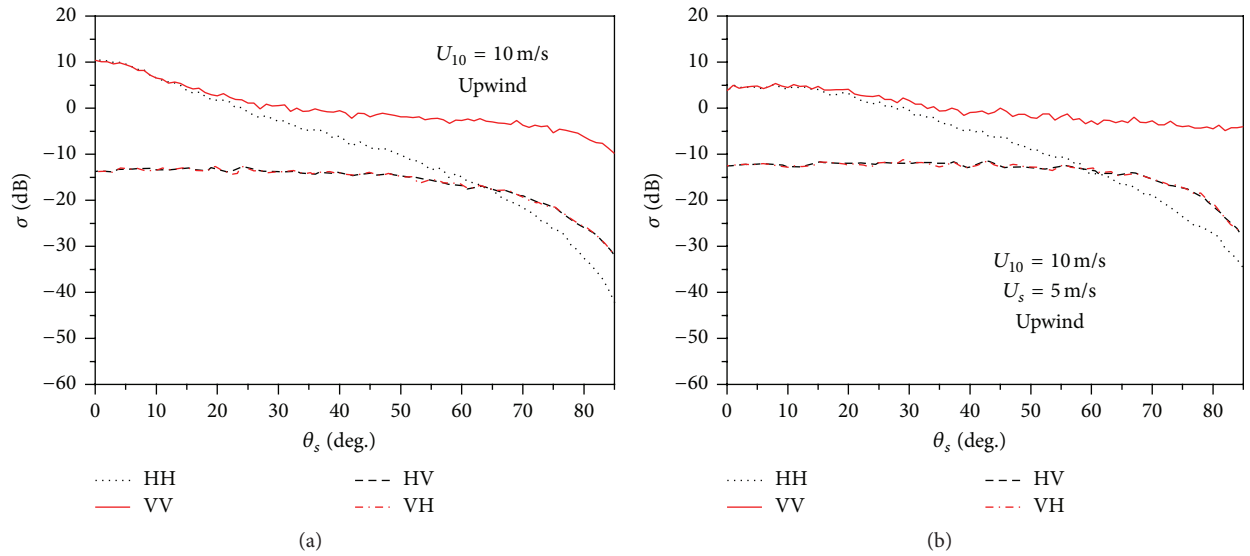

FIGURE 6: Similar to Figure 5, but for wind speed U_{10} = 10 m/s. (a) Sea surface only and (b) sea surface with wake at ship speed U_s = 5 m/s.

comparing Figures 5(b) and 6(b), it is indicated that, for sea surface with ship-induced Kelvin wake with ship speed U_s = 5 m/s, the scattering intensity near normal incidence for wind speed U_{10} = 10 m/s is approximately equally to that for wind speed U_{10} = 3 m/s. This is due mainly to the fact that, under wind speed U_{10} = 10 m/s, the contribution of ship-induced wake is very small.

To illustrate the effect of a ship's Kelvin wake on copolarized backscattering coefficient, in Figures 7(a) and 7(b) we make a comparison of the copolarized backscattering coefficient from 2D rough sea surface with and without a ship's Kelvin wake embedded in it for ship speeds U_s = 3 m/s and U_s = 5 m/s, respectively. The wind speed is U_{10} = 3 m/s. In Figures 7(a) and 7(b), the copolarized backscattering coefficient from rough sea surface with an embedded ship's Kelvin wake is significantly weaker than that from sea surface without an embedded wake in the vicinity of the normal incidence. Moreover, the backscattering coefficient from sea surface with an embedded ship's Kelvin wake is weaker for ship speed U_s = 5 m/s than for ship speed U_s = 3 m/s near the normal incidence. As the incident angle increases, there is a slight difference between the backscattering coefficient from rough sea surface with and without an embedded ship's Kelvin wake for ship speed U_s = 3 m/s, and the backscattering coefficient from sea surface with a ship's Kelvin wake becomes stronger than that from sea surface without a ship's Kelvin wake with ship speed U_s = 5 m/s especially for HH-polarization. This means that the backscattering from

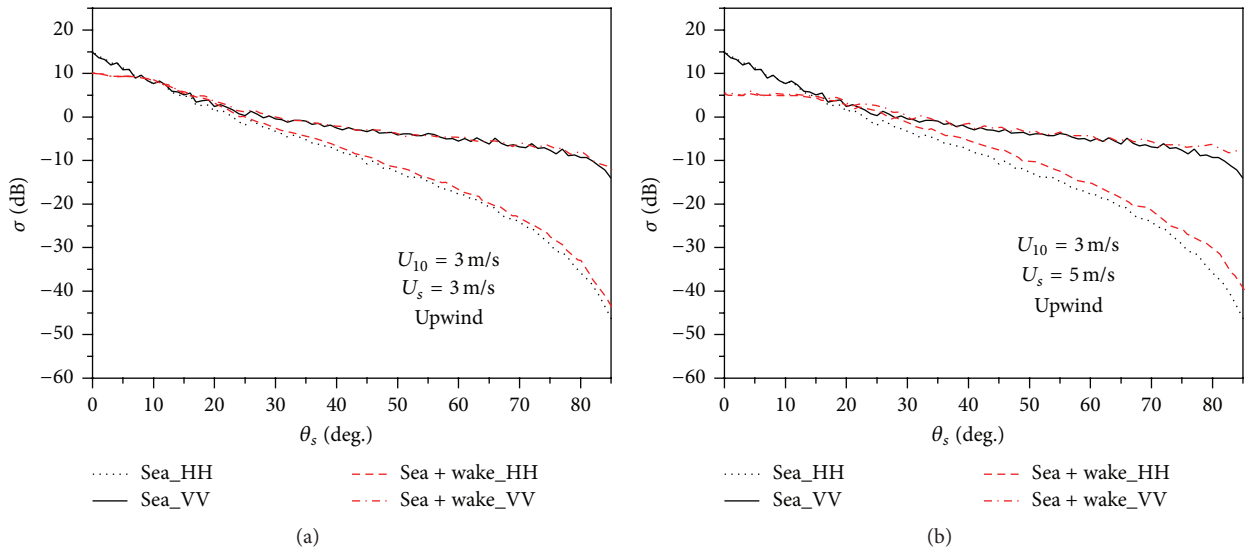

FIGURE 7: Comparison of copolarized backscattering coefficient from 2D rough sea surface with and without an embedded ship-induced Kelvin wake with wind speed $U_{10} = 3$ m/s. (a) Ship speed $U_s = 3$ m/s and (b) ship speed $U_s = 5$ m/s.

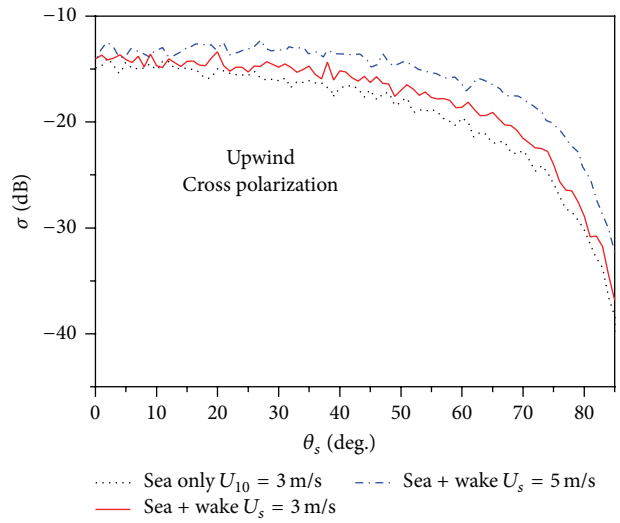

FIGURE 8: Cross-polarized backscattering coefficient from 2D rough sea surface with and without an embedded ship's Kelvin wake with wind speed $U_{10} = 3$ m/s.

sea surface in the presence of a ship's Kelvin wake is enhanced away from the normal incidence due to the existence of ship's Kelvin wake. We attribute this phenomenon to the fact that, under a low wind speed $U_{10} = 3$ m/s, the presence of a ship's Kelvin wake makes the sea surface roughness increase, and a higher ship speed $U_s = 5$ m/s makes the background consisting of sea surface and ship's Kelvin wake much rougher compared with a lower ship speed $U_s = 3$ m/s.

Figure 8 exhibits the cross-polarized backscattering coefficient from sea surface with and without an embedded ship's Kelvin wake. To better illustrate the effect of a ship's Kelvin wake on the cross-polarized backscattering coefficient, the wind speed is fixed at $U_{10} = 3$ m/s. Two typical ship-induced Kelvin wakes with ship speeds $U_s = 3$ m/s and $U_s = 5$ m/s are considered in Figure 8. As expected, the ship's Kelvin wake plays an important role in the depolarization of wave scattering from rough surface. The depolarized backscattering coefficient from sea surface with an embedded ship's Kelvin wake is stronger than that without wake. Moreover, under a fixed wind speed $U_{10} = 3$ m/s, the depolarized backscattering coefficient from sea surface with an embedded ship's Kelvin wake is larger for ship speed $U_s = 5$ m/s than for ship speed $U_s = 3$ m/s. This is attributed to the fact that sea surface roughness becomes larger due to the presence of an embedded ship's Kelvin wake and that sea surface roughness grows larger as the ship speed increases under a low wind speed $U_{10} = 3$ m/s. What is more, the depolarization of wave scattering from rough surface is due to multiple scattering and a rougher sea surface leads to a stronger multiple scattering. It should be mentioned that Fung and Eom [7] investigated the multiple scattering and depolarization by Kirchhoff approximation and pointed out that the copolarized backscattering is dominated by the single scattering process, whereas the depolarized backscattering is due to multiple scattering. Thus, we can speculate that, under a fixed sea surface wind speed, a higher ship speed will give rise to a stronger depolarized scattering.

Figures 9(a) and 9(b) present a comparison of the angular distribution of bistatic scattering coefficient with and without an embedded ship's Kelvin wake with incident angle $\theta_i = 0^\circ$ for HH- and VV-polarization, respectively. To better illustrate the effect of a ship's Kelvin wake, the wind speed is fixed at $U_{10} = 3$ m/s. Two typical ship-generated Kelvin wakes with ship speeds $U_s = 3$ m/s and $U_s = 5$ m/s are considered here. In Figure 10, the incident angle is $\theta_i = 60^\circ$, and other parameters are the same as in Figure 9. From

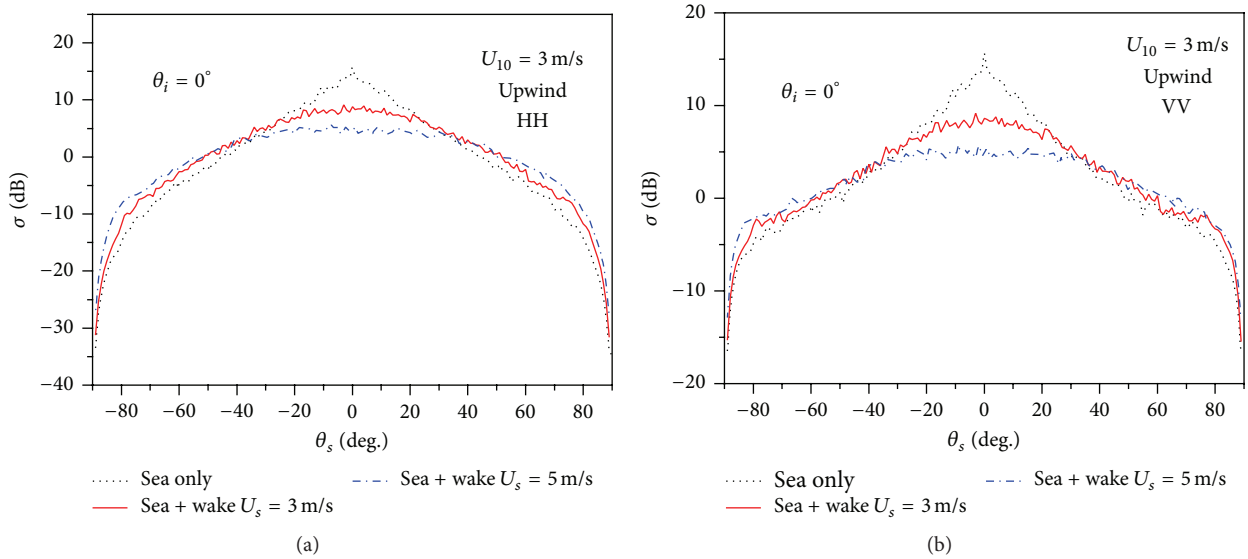

FIGURE 9: The angular distribution of bistatic scattering coefficient with and without an embedded ship's Kelvin wake at a fixed wind speed $U_{10} = 3$ m/s. (a) HH-polarization and (b) VV-polarization.

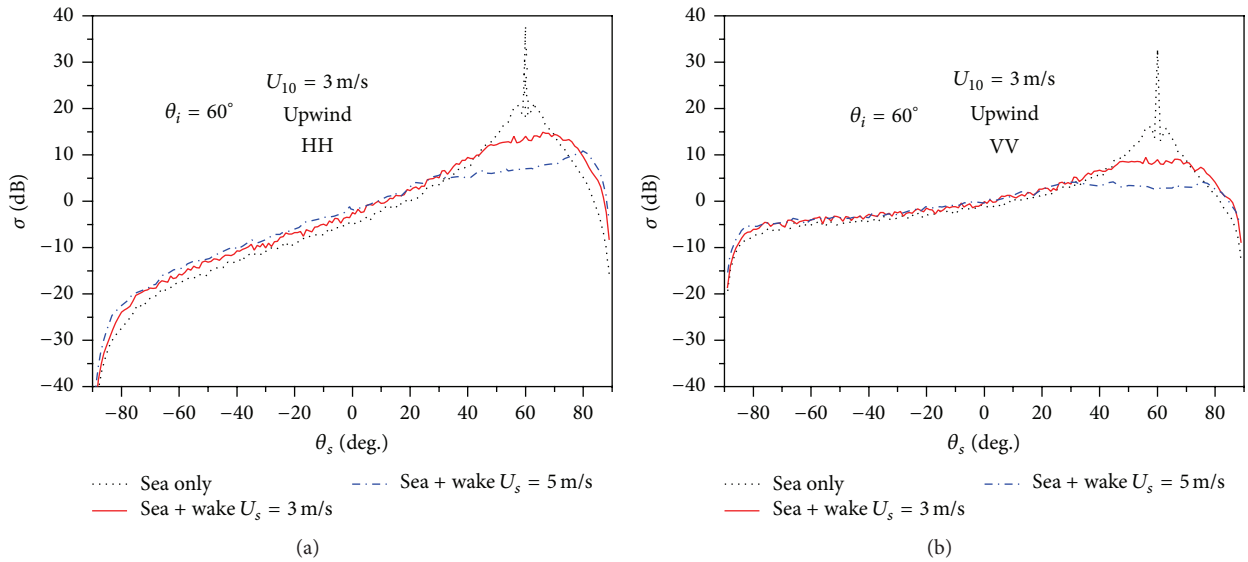

FIGURE 10: Similar to Figure 9, but with incident angle $\theta_i = 60^\circ$. (a) HH-polarization and (b) VV-polarization.

Figures 9 and 10, we can readily observe obvious peaks in the specular direction for sea surface without an embedded ship's Kelvin wake. This is attributed to the fact that the coherent scattering is very strong and the scattering mechanism is dominated by specular reflection. Hence, a coherent sharp peak appears at low wind conditions. We can expect that this sharp peak disappears if the coherent component was subtracted. The angular distribution of bistatic scattering intensity in the specular direction is strongly influenced by the ship's Kelvin wake, and this difference is relatively small away from the specular direction. We can speculate that, under a fixed wind speed $U_{10} = 3$ m/s, the scattering intensity in the specular direction becomes weaker with the ship speed increasing due to the increase of sea surface roughness. A backscattering enhancement is observed by comparing the scattering coefficient from sea surface with and without a ship's Kelvin wake. Moreover, a larger ship speed gives rise to a stronger backscattering enhancement under a fixed wind speed $U_{10} = 3$ m/s. We conclude here that when the sea surface wind speed is sufficiently high until the ship's Kelvin wake is submerged in sea surface, the scattering contribution comes primarily from sea surface itself and that the ship's

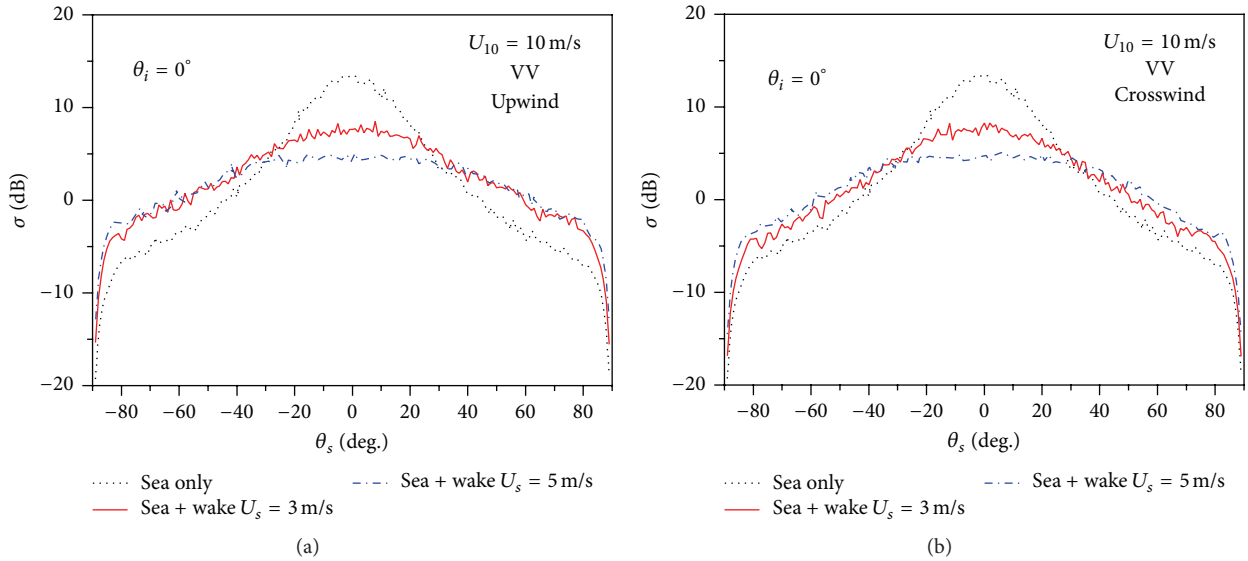

FIGURE 11: The angular distribution of bistatic scattering coefficient of sea surface with and without a ship-induced kelvin wake for VV-polarization at wind speed U_{10} = 10 m/s. (a) Upwind case and (b) crosswind case.

Kelvin wake begins to contribute to scattering as the ship speed increases under low wind conditions.

The angular distribution of bistatic scattering coefficient of sea surface with and without a ship-induced Kelvin wake for VV-polarization at speed U_{10} = 10 m/s is presented in Figures 11(a) and 11(b) for upwind case and crosswind case, respectively. We can observe from Figure 11 that, due to the presence of a ship-induced Kelvin wake, the scattering intensity of sea surface in the specular direction is decreased and the backscattering is enhanced. Moreover, under a fixed wind speed U_{10} = 10 m/s, the scattering intensity in the specular direction decreases with ship speed increasing. This is attributed to the fact that sea surface becomes rougher due to the presence of ship wake and that under a fixed wind speed a higher ship speed gives rise to a larger roughness. Comparing Figures 11(a) and 11(b), we can observe that it is not easy to observe significant difference between upwind case and crosswind case. In the following, we will discuss the dependence of bistatic scattering coefficient of sea surface with and without wake on the scattering azimuth angle.

From Figures 9, 10, and 11, we can observe that the scattering intensity near the specular direction is significantly influenced due to the presence of ship-induced wake, even for higher wind speed and lower ship speed as depicted in Figure 11. However, the influence of ship wake on the scattering coefficient away from the specular direction is relatively small, especially for oblique incidence as illustrated in Figure 10. In comparison with bistatic configuration, the backscattering coefficient away from specular direction is less sensitive to ship-induced wake as illustrated in Figure 7. From Figure 7, we can observe that, even at low wind condition U_{10} = 3 m/s, the backscattering scattering coefficient away from the specular direction is not significantly affected by ship wake at ship speeds U_s = 3 m/s and U_s = 5 m/s. This implies that, for monostatic configuration even at low wind condition U_{10} = 3 m/s, the ship wake contribution on the backscattering coefficient away from the specular direction is negligible under low ship speed conditions. It should be noted that these conclusions are drawn with the fixed ship parameters. The influence of other parameters such as ship size on the angular distribution of scattering coefficient is not conducted in this paper due to space limitation, which deserves further investigation.

Figures 12(a) and 12(b) show the angular distribution of bistatic polarimetric scattering coefficient with incident angle $\theta_i = 0^\circ$ for sea surface with and without an embedded ship's Kelvin wake, respectively. The wind speed is fixed at U_{10} = 3 m/s, and the ship speed is U_s = 5 m/s. In Figure 13, the incident angle is $\theta_i = 60^\circ$, and other parameters are the same as Figure 12. In Figures 12(a) and 13(a), obvious peaks appear for copolarized scattering coefficient in the specular direction. When a ship's Kelvin wake is embedded in sea surface, however, the specular peaks disappear as depicted in Figures 12(b) and 13(b). This can be attributed to the fact that the coherent scattering in the specular direction is weakened due to the presence of ship's Kelvin wake. In Figures 12 and 13, we can readily observe that the copolarized scattering intensity is significantly stronger than the cross-polarized one in the vicinity of the specular direction, whereas their difference is small far away from the specular direction as depicted in Figure 13. By comparing Figure 12(a) with Figure 12(b) and Figure 13(a) with Figure 13(b), we find that the cross-polarized bistatic scattering coefficient is larger for sea surface with an embedded ship's Kelvin wake than for sea surface without wake. We attribute this phenomenon to the fact that the depolarized scattering becomes stronger, which is a result of multiple scattering arising from a larger sea surface roughness due to the presence of a ship's Kelvin wake.

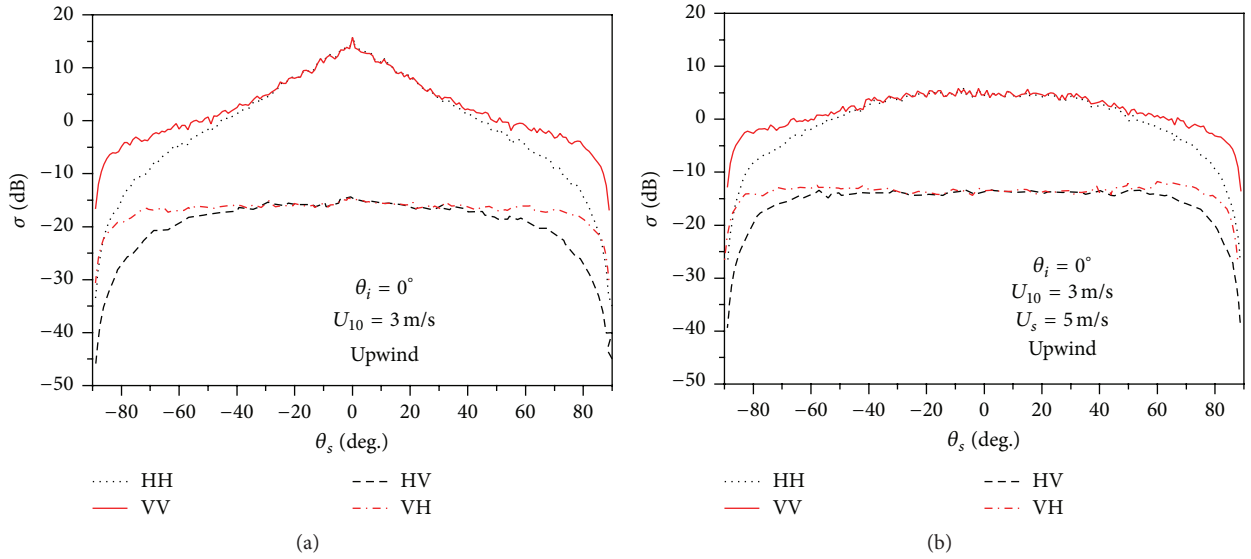

FIGURE 12: Bistatic polarimetric scattering coefficient versus scattering angle θ_s with wind speed $U_{10} = 3$ m/s for incident angle $\theta_i = 0^\circ$. (a) Sea alone and (b) sea with wake.

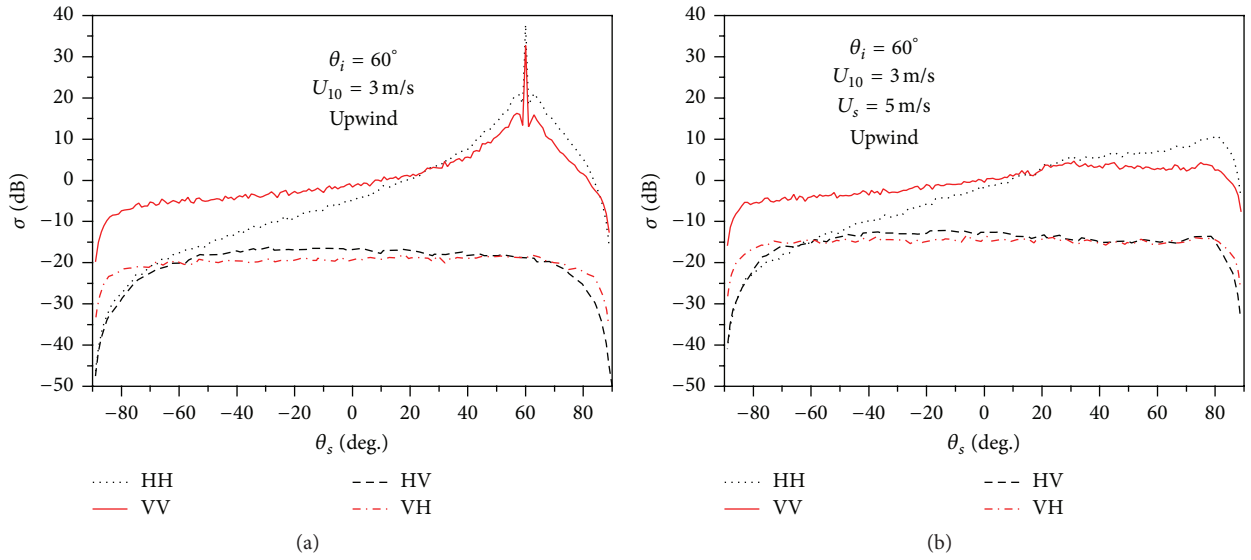

FIGURE 13: Similar to Figure 12, but with incident angle $\theta_i = 60^\circ$. (a) Sea alone and (b) sea with wake.

By the way, for a bistatic configuration, the reciprocity is not obeyed since the HV-polarized scattering coefficient is not equal to the VH-polarized one as depicted in Figures 12 and 13, which is different from the monostatic configuration.

Figure 14 makes a comparison of bistatic scattering coefficient versus scattering azimuth angle of the simulation result in this paper with the result published in [25]. In Figure 14, the simulations are performed at 14 GHz. The incidence angle and incidence azimuth angle are $\theta_i = 40^\circ$ and $\phi_i = 0^\circ$, respectively. The scattering angle is $\theta_s = 40^\circ$. From Figure 14, we can observe that the variation tendency of our simulation result is consistent with the results published in [25]. The comparison shows that the scattering coefficient of this paper is somewhat smaller than that published in [25], especially at small scattering azimuth angles. However, the scattering coefficient of this paper, in principle, should be slightly larger than that published in [25]. The reason is that the SSA-II is adopted in the present study in which a second-order correction is added to SSA-I, while in [25] the SSA-I is utilized. The possible reasons leading to this discrepancy could be the following simulation condition differences. For example, the sea surface size in this paper is very limited

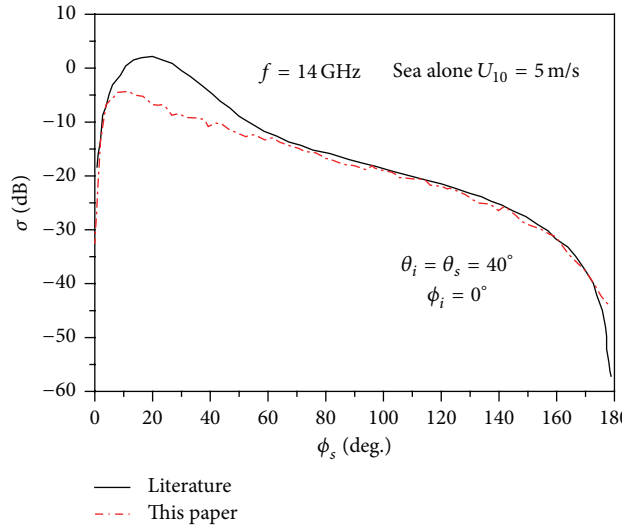

Figure 14: Comparison of bistatic scattering coefficient versus scattering azimuth angle.

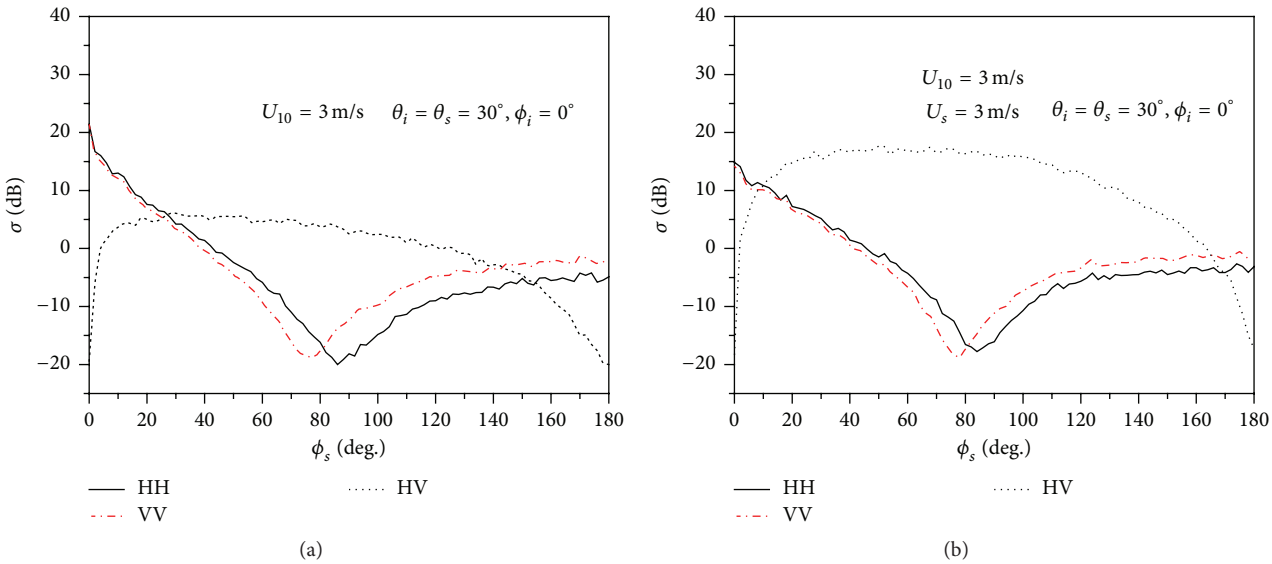

Figure 15: Bistatic scattering coefficient versus scattering azimuth angle ϕ_s. (a) Sea surface alone at wind speed $U_{10} = 3$ m/s and (b) sea surface with ship wake at wind speed $U_{10} = 3$ m/s and ship speed $U_s = 5$ m/s.

due to the severe computational burden involved in SSA-II, whereas sea surface size is assumed to be infinite in [25]. The wind fetch involved in Elfouhaily et al. spectrum [28] is set as $X = 30$ km in the present study, and it seems as if the value of wind fetch is not explicitly specified in [25]. In addition, the scattering coefficient of this paper is obtained over 100 sea surface realizations, whereas the statistical solution of scattering coefficient is presented in [25].

The variation of bistatic scattering coefficient with scattering azimuth angle is presented in Figures 15(a) and 15(b) for sea surface only and sea surface with a ship-induced Kelvin wake, respectively. In Figure 15, the incidence angle and incidence azimuth angle are $\theta_i = 30^\circ$ and $\phi_i = 0^\circ$, respectively. The scattering angle is $\theta_s = 30^\circ$. In Figure 16, all simulation parameters are the same as those in Figure 15, but with incidence angle $\theta_i = 40^\circ$ and scattering angle $\theta_s = 40^\circ$. From Figures 15 and 16, we can observe that the copolarized scattering coefficient encounters a minimum when scattering azimuth angle varies from 0° to 180°. More specifically, for HH-polarization, the minimum of scattering coefficient appears in the vicinity of scattering orthogonal plane ($\phi_s = 90^\circ$). However, we can notice that for VV-polarization the position of the minimum of scattering coefficient depends on the value of incidence/scattering angle. Similar conclusions were reported in [25], in which the statistical solution of sea surface scattering is obtained by using first-order small-slope

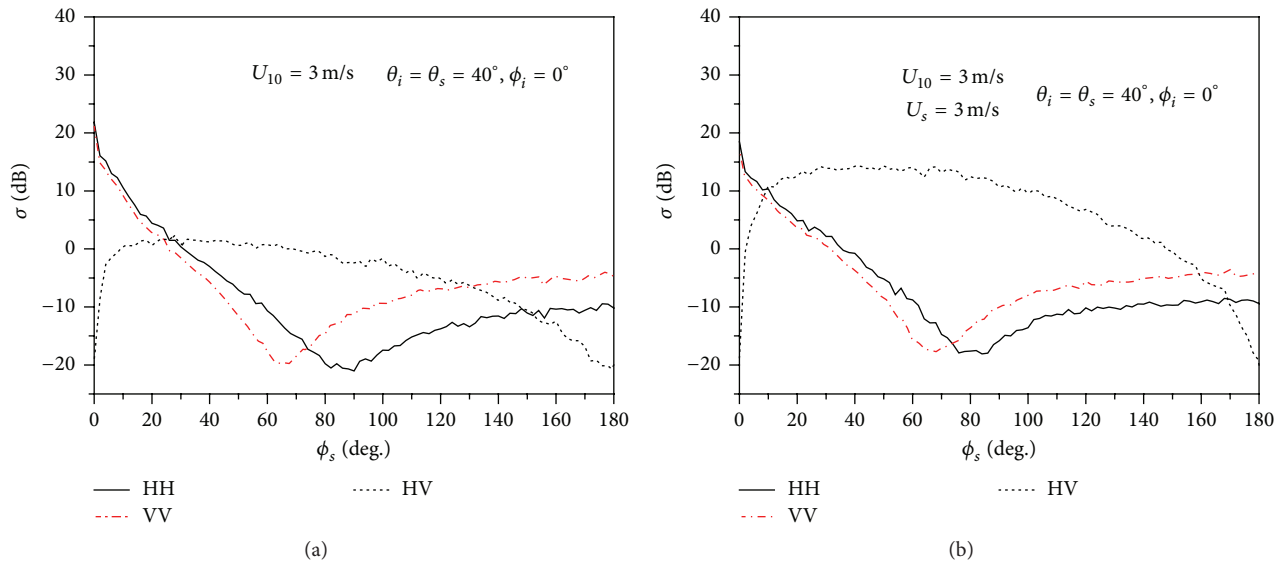

FIGURE 16: Similar to Figure 15, but with incidence angle $\theta_i = 40^\circ$ and scattering angle $\theta_s = 40^\circ$. (a) Sea surface alone at wind speed $U_{10} = 3$ m/s and (b) sea surface with ship wake at wind speed $U_{10} = 3$ m/s and ship speed $U_s = 5$ m/s.

approximation. Comparing Figure 15(a) with Figure 15(b) and Figure 16(a) with Figure 16(b), we can observe that the cross-polarized scattering coefficient of sea surface with a ship-induced wake is obviously larger than that of sea surface alone. That is, the depolarized scattering is enhanced due to the presence of ship-induced Kelvin wake. This is attributed to the fact that sea surface in the presence of ship-induced wake is much rougher than sea surface alone. Thus, we can expect that the enhanced depolarized scattering due to the presence of a ship-induced kelvin wake is potentially valuable for the detection of ships in marine environment.

5. Conclusion

In this paper, fully polarimetric monostatic and bistatic scattering from rough sea surface in the presence of a ship's Kelvin wake has been investigated in detail by comparison with that from single sea surface without ship-induced Kelvin wake. For bistatic configuration, the copolarized scattering intensity is significantly stronger than the cross-polarized one in the vicinity of the specular direction, whereas this difference is small far away from the specular direction. Meanwhile, the copolarized backscattering coefficient is much stronger than the cross-polarized one except for the larger incident angles. The numerical simulations show that the ship speed is an important parameter for influencing the radar echo signatures, since the sea surface roughness depends mainly on the ship speed with fixed ship parameters under low wind conditions. It is also indicated that a larger ship speed gives rise to a stronger enhanced backscattering and enhanced depolarized scattering under low wind conditions, which is a result of multiple scattering arising from a larger sea surface roughness due to the presence of a ship's Kelvin wake. It should be noted that the dependence of angular distribution of scattering intensity on ship parameters is not examined in the present study due to space limitation. However, we can speculate that ship parameters can also affect the radar echo signatures, since a ship's Kelvin wake also depends on the ship parameters such as ship length, beam, and draft. The investigation of polarimetric scattering from rough ocean surface in the presence of ship-induced Kelvin wake is potentially valuable for the detection and classification of ships in marine environment. It should be pointed out that SAR imaging simulation of sea surface with an embedded ship-induced Kelvin wake based on simulated electromagnetic scattering data deserves further investigation, which goes beyond the scope of this paper.

Conflict of Interests

The authors declare that there is no conflict of interests regarding the publication of this paper.

Acknowledgments

This work was supported by the National Science Foundation for Distinguished Young Scholars of China (Grant no. 61225002), partially by the National Natural Science Funds (Grant no. 41406201), and the Scientific Research Program Funded by Shaanxi Provincial Education Department (no. 15JK1180).

References

[1] K. Eldhuset, "An automatic ship and ship wake detection system for spaceborne SAR images in coastal regions," *IEEE Transactions on Geoscience and Remote Sensing*, vol. 34, no. 4, pp. 1010–1019, 1996.

[2] G. Zilman, A. Zapolski, and M. Marom, "The speed and beam of a ship from its wake's SAR images," *IEEE Transactions on*

Geoscience and Remote Sensing, vol. 42, no. 10, pp. 2335–2343, 2004.

[3] J. K. E. Tunaley, E. H. Buller, K. H. Wu, and M. T. Rey, "The simulation of the SAR image of a ship wake," *IEEE Transactions on Geoscience and Remote Sensing*, vol. 29, no. 1, pp. 149–156, 1991.

[4] K. Oumansour, Y. Wang, and J. Saillard, "Multifrequency SAR observation of a ship wake," *IEE Proceedings-Radar Sonar and Navigation*, vol. 143, no. 4, pp. 275–280, 1996.

[5] A. Arnold-Bos, A. Khenchaf, and A. Martin, "Bistatic radar imaging of the marine environment. Part II. Simulation and results analysis," *IEEE Transactions on Geoscience and Remote Sensing*, vol. 45, no. 11, pp. 3384–3396, 2007.

[6] G. Zilman, A. Zapolski, and M. Marom, "On detectability of a ship's Kelvin wake in simulated SAR images of rough sea surface," *IEEE Transactions on Geoscience and Remote Sensing*, vol. 53, no. 2, pp. 609–619, 2015.

[7] A. K. Fung and H. J. Eom, "Multiple scattering and depolarization by a randomly rough Kirchhoff surface," *IEEE Transactions on Antennas and Propagation*, vol. 29, no. 3, pp. 463–471, 1981.

[8] D. Miret, G. Soriano, and M. Saillard, "Rigorous simulations of microwave scattering from finite conductivity two-dimensional sea surfaces at low grazing angles," *IEEE Transactions on Geoscience and Remote Sensing*, vol. 52, no. 6, pp. 3150–3158, 2014.

[9] D. Z. Ding, G. M. Li, Y. Y. An, and R. S. Chen, "Application of hierarchical two-level spectral preconditioning method for electromagnetic scattering from the rough surface," *International Journal of Antennas and Propagation*, vol. 2014, Article ID 752418, 10 pages, 2014.

[10] H. Chen, M. Zhang, and H.-C. Yin, "Facet-based treatment on microwave bistatic scattering of three-dimensional sea surface with electrically large ship," *Progress in Electromagnetics Research*, vol. 123, pp. 385–405, 2012.

[11] F. Xu and Y.-Q. Jin, "Bidirectional analytic ray tracing for fast computation of composite scattering from electric-large target over a randomly rough surface," *IEEE Transactions on Antennas and Propagation*, vol. 57, no. 5, pp. 1495–1505, 2009.

[12] Y. Zhao, X.-F. Yuan, M. Zhang, and H. Chen, "Radar scattering from the composite ship-ocean scene: facet-based asymptotical model and specular reflection weighted model," *IEEE Transactions on Antennas and Propagation*, vol. 62, no. 9, pp. 4810–4815, 2014.

[13] A. Bausssard, M. Rochdi, and A. Khenchaf, "PO/MEC-based scattering model for complex objects on a sea surface," *Progress in Electromagnetics Research*, vol. 111, pp. 229–251, 2011.

[14] R. Wang, S.-R. Chai, and L.-X. Guo, "Fast hybrid method for the study on monostatic scattering from plasma-coated target above a rough surface," *International Journal of Antennas and Propagation*, vol. 2014, Article ID 762603, 13 pages, 2014.

[15] R.-Q. Sun, M. Zhang, C. Wang, and Y. Chen, "Study of electromagnetic scattering from ship wakes on PEC sea surfaces by the small-slope approximation theory," *Progress in Electromagnetics Research*, vol. 129, pp. 387–404, 2012.

[16] H. J. Luo, G. D. Yang, Y. H. Wang, J. C. Shi, and Y. Du, "Numerical studies of sea surface scattering with the GMRES-RP method," *IEEE Transactions on Geoscience and Remote Sensing*, vol. 52, no. 4, pp. 2064–2073, 2014.

[17] C. G. Jia, L. X. Guo, and P. J. Yang, "EM scattering from a target above a 1-D randomly rough sea surface using GPU-based parallel FDTD," *IEEE Antennas and Wireless Propagation Letters*, vol. 14, pp. 217–220, 2015.

[18] A. Khenchaf, "Bistatic scattering and depolarization by randomly rough surfaces: application to the natural rough surfaces in X-band," *Waves Random Media*, vol. 11, no. 2, pp. 61–89, 2001.

[19] P. Beckmann and A. Spizzichino, *The Scattering of Electromagnetic Waves from Rough Surfaces*, Pergamon Press, Oxford, UK, 1963.

[20] L. Tsang, J. A. Kong, and K. H. Ding, *Scattering of Electromagnetic Waves: Theories and Applications*, vol. 1, Wiley-Interscience, New York, NY, USA, 1st edition, 2000.

[21] L. Tsang and J. A. Kong, *Scattering of Electromagnetic Waves: Advanced Topics*, vol. 3, Wiley-Interscience, New York, NY, USA, 2001.

[22] F. T. Ulaby, R. K. Moore, and A. K. Fung, *Microwave Remote Sensing: Active and Passive Volume II: Radar Remote Sensing and Surface Scattering and Emission Theory*, vol. 2, Addison-Wesley, Reading, Mass, USA, 1982.

[23] M. Y. Ayari, A. Khenchaf, and A. Coatanhay, "Simulations of the bistatic scattering using two-scale model and the unified sea spectrum," *Journal of Applied Remote Sensing*, vol. 1, no. 1, Article ID 013532, 2007.

[24] G. R. Valenzuela, "Depolarization of EM waves by slightly rough surfaces," *IEEE Transactions on Antennas and Propagation*, vol. 15, no. 4, pp. 552–557, 1967.

[25] A. Awada, M. Y. Ayari, A. Khenchaf, and A. Coatanhay, "Bistatic scattering from an anisotropic sea surface: numerical comparison between the first-order SSA and the TSM models," *Waves in Random and Complex Media*, vol. 16, no. 3, pp. 383–394, 2006.

[26] A. Awada, A. Khenchaf, and A. Coatanhay, "Bistatic radar scattering from an ocean surface at L-band," in *Proceedings of the IEEE Radar Conference*, pp. 200–207, Verona, NY, USA, April 2006.

[27] A. G. Voronovich and V. U. Zavorotny, "Full-polarization modeling of monostatic and bistatic radar scattering from a rough sea surface," *IEEE Transactions on Antennas and Propagation*, vol. 62, no. 3, pp. 1362–1371, 2014.

[28] T. Elfouhaily, B. Chapron, K. Katsaros, and D. Vandemark, "A unified directional spectrum for long and short wind-driven waves," *Journal of Geophysical Research*, vol. 102, no. 7, pp. 15781–15796, 1997.

[29] A. G. Voronovich, *Wave Scattering from Rough Surfaces*, Springer, Berlin, Germany, 2nd edition, 1999.

[30] D. Nie, M. Zhang, and N. Li, "Investigation on microwave polarimetric scattering from two-dimensional wind fetch- and water depth-limited nearshore sea surfaces," *Progress in Electromagnetics Research*, vol. 145, pp. 251–261, 2014.

[31] L. Tsang, J. A. Kong, K. Ding, and C. O. Ao, *Scattering of Electromagnetic Waves: Numerical Simulations*, vol. 2, John Wiley & Sons, New York, NY, USA, 2001.